

Supplementary Materials for

**Physically defined long-term and short-term synapses for the development of reconfigurable analog-type operators capable of performing health care tasks**

Yongsuk Choi *et al.*

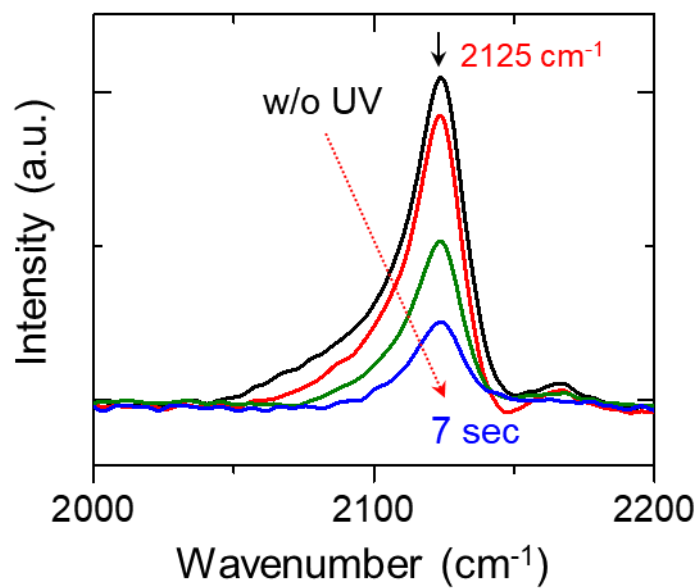
Corresponding author: Wei Gao, [weigao@caltech.edu](mailto:weigao@caltech.edu); Jeong Ho Cho, [jhcho94@yonsei.ac.kr](mailto:jhcho94@yonsei.ac.kr)

*Sci. Adv.* **9**, eadg5946 (2023)  
DOI: 10.1126/sciadv.adg5946

**This PDF file includes:**

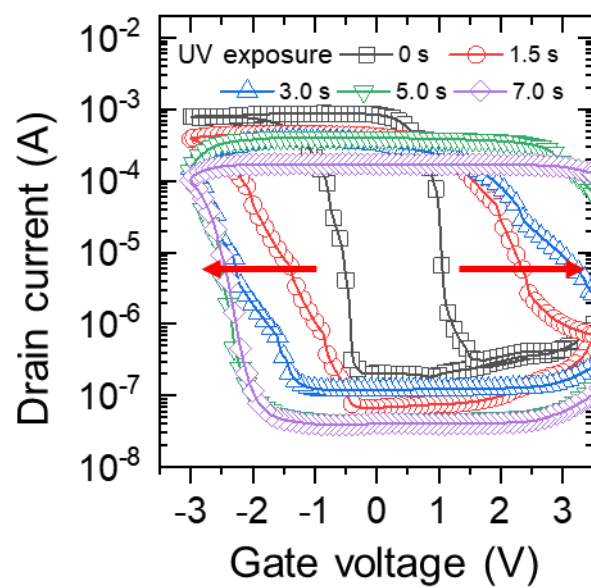
Figs. S1 to S14

## Supplementary Figures



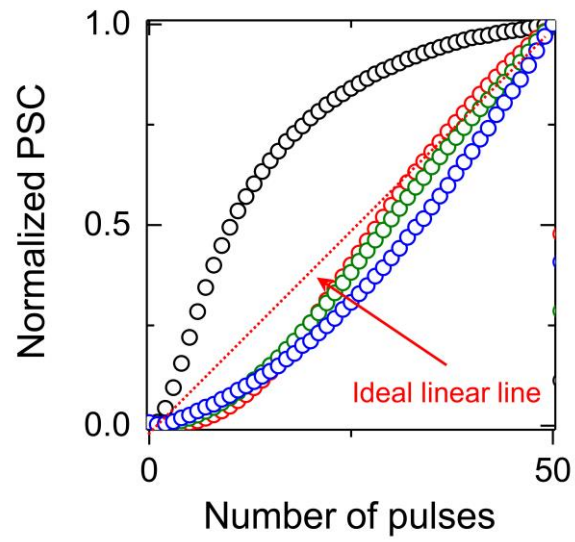
### Supplementary Fig. S1 | Confirmation of the photochemical reaction.

Fourier transform infrared (FTIR) spectroscopy of P3HT under varied UV irradiation time from 0 to 7 s. The peak appears at 2125 cm<sup>-1</sup> is originated from the N≡N stretching vibration in the azide group.

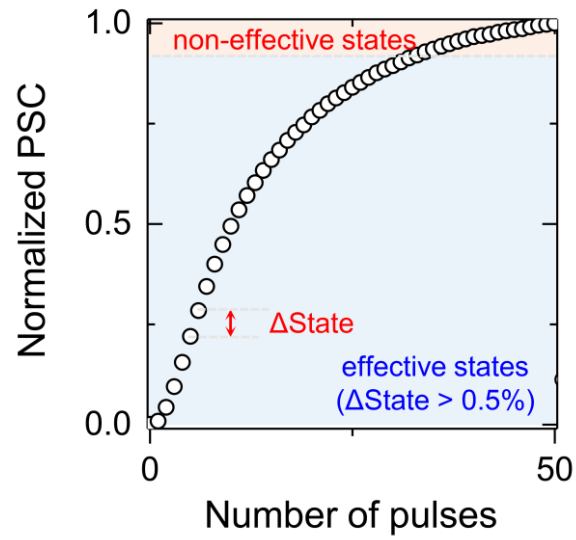


**Supplementary Fig. S2 | Confirmation of ion-penetration behavior by tracking hysteresis behavior as function of the reaction time.**

Typical transfer characteristics (PSC- $V_{WC}$  curve) of vertical synapse with varied UV exposure time.

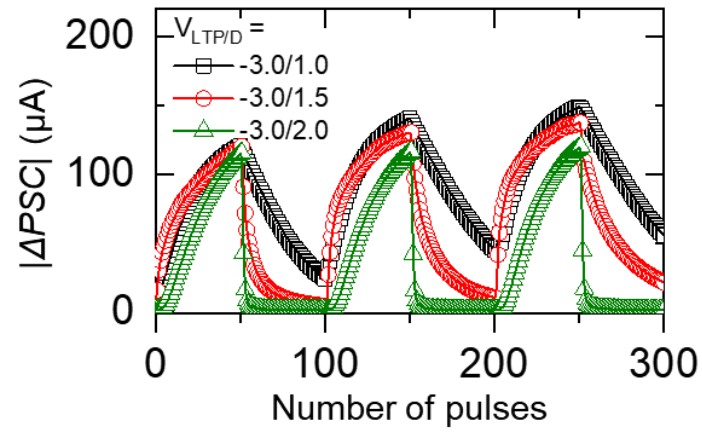


**Supplementary Fig. S3 | Normalized PSC states in the LTP curve.**  
Measured(dots) and ideal linear line plots from LTP curves of **Fig. 3d**.



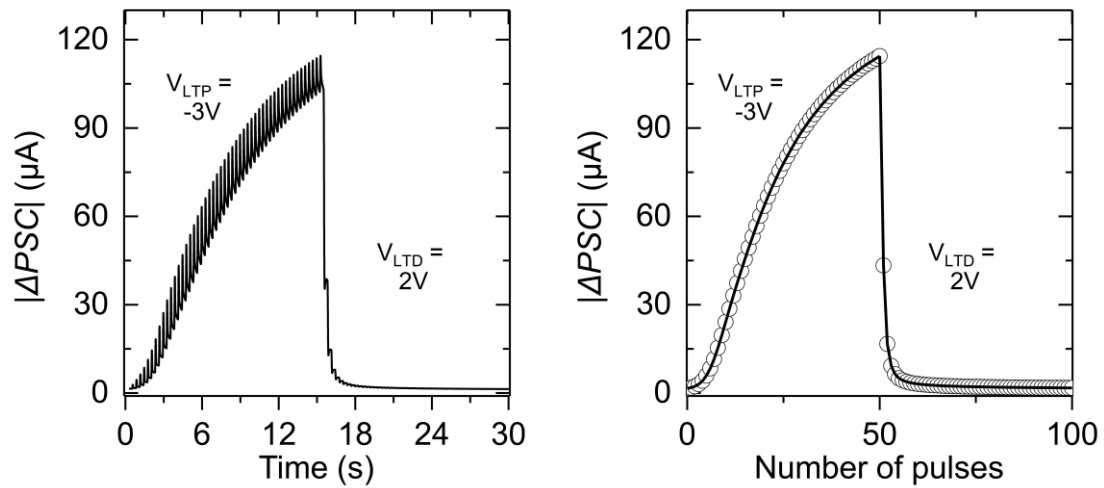
**Supplementary Fig. S4 | Method for calculation of the effective number of states.**

The normalized PSC states with the dynamic range were plotted as a function of pulse number. And then, the states having  $\Delta\text{state}$  above the 0.5% of the dynamic range were defined as the effective states.



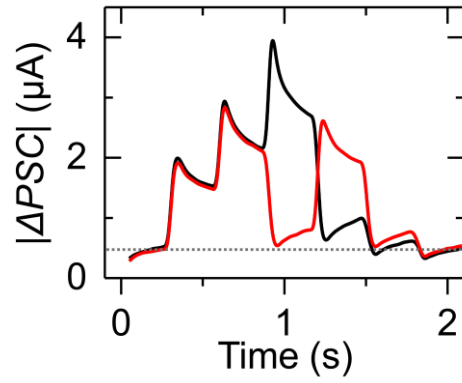
**Supplementary Fig. S5 | LTP/D curves under varied depression voltage pulses.**

Among the varied depression voltages for the LTP/D measurement, the  $V_{LTD}$  of 2V showed the most reliable reset property.



**Supplementary Fig. S6 | Extraction of representative PSC state from real-time LTP/D curve.**

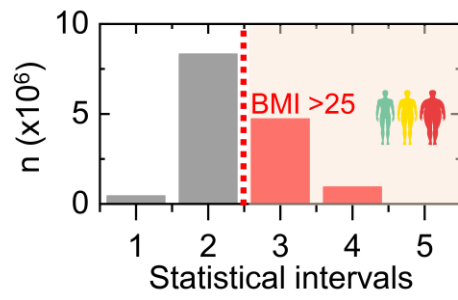
The LTP/D curve has 50 potentiation and 50 depression cycles, and each update cycle consists of 10 data points. The first data point represents the current upon pulse input, and the remaining 9 data points represent the following retention current. The last data point of the cycle, the point before the following pulse input, is defined as a representative PSC state.



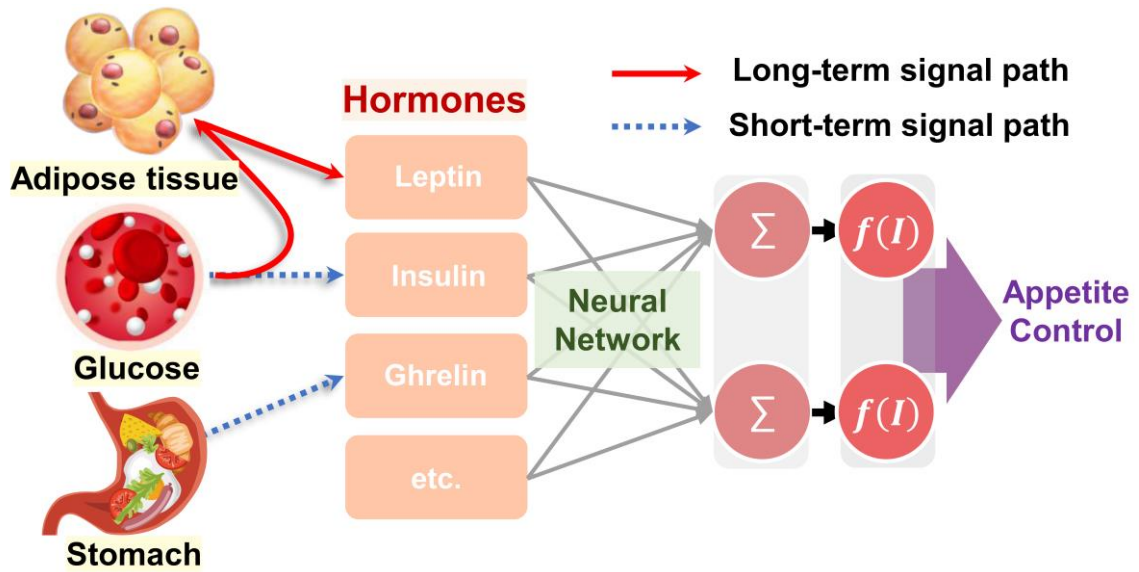
**Supplementary Fig. S7 | Verification of state stability by overlapping of PSC responses from regular and irregular pulse updates.**

The regular pulse set consists of consecutive 3 potentiation pulses followed by 3 depression pulses(PPPDDD) while the irregular pulse set has the mixed ordering of potentiation and depression pulses(PPDPDD).



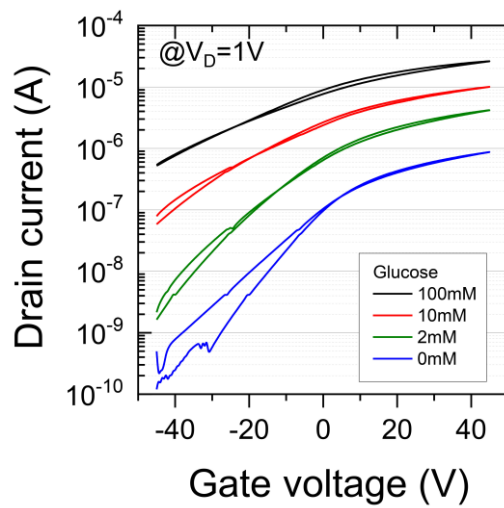


**Supplementary Fig. S8 | Pre-recorded statistical data for reconfigurable synaptic logic operation.**  
Distributions of body mass index (BMI) for the Korean population in 2020 by a statistical interval.



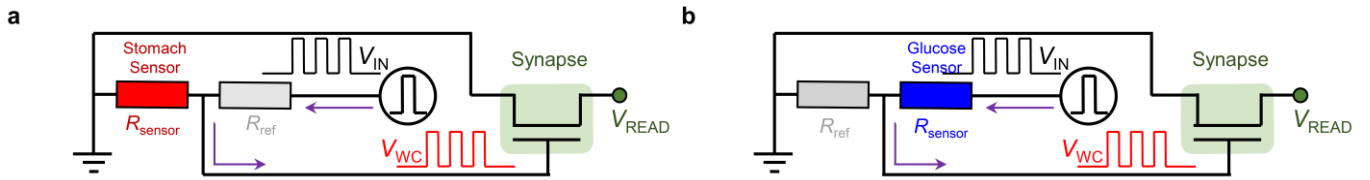
**Supplementary Fig. S9 | Schematic diagram of the human appetite controlling system.**

Neural signals transmitted through hormones from each cell and tissue are integrated and processed through a biological neural network to control appetite.



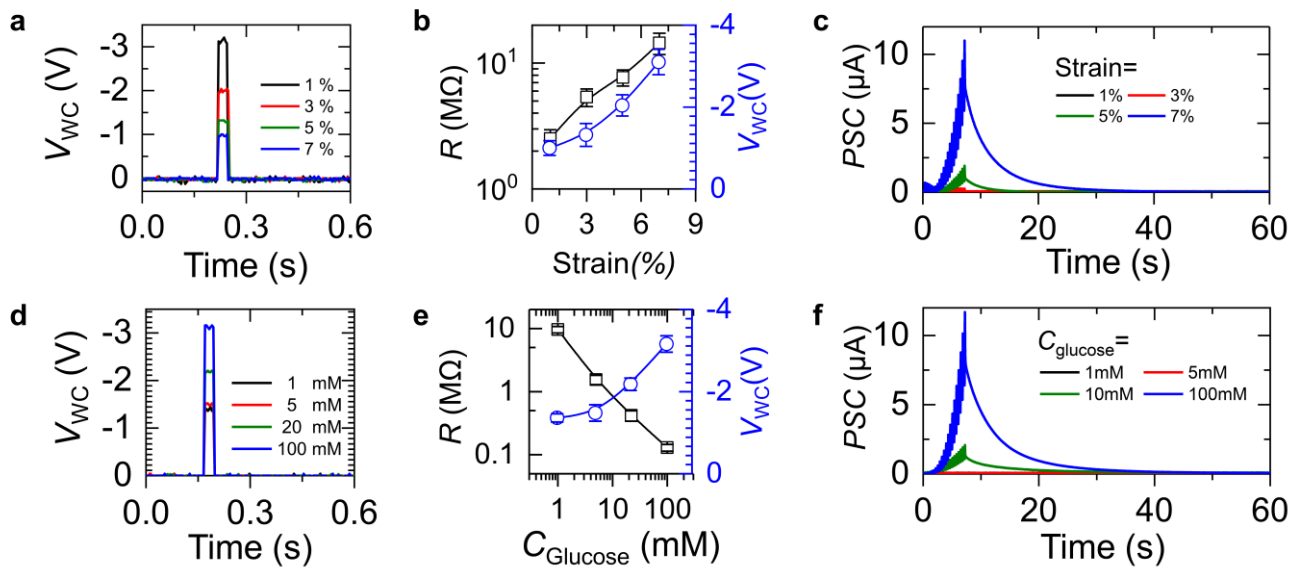
**Supplementary Fig. S10 | Transfer curves of an indium gallium zinc oxide (IGZO) transistor under varying glucose concentrations.**

The IGZO transistor was fabricated on SiO<sub>2</sub>/Si<sup>++</sup> wafer and the test solution containing glucose was dropped on the channel. The gate voltage was applied through the 100-nm-thick SiO<sub>2</sub> dielectric layer.



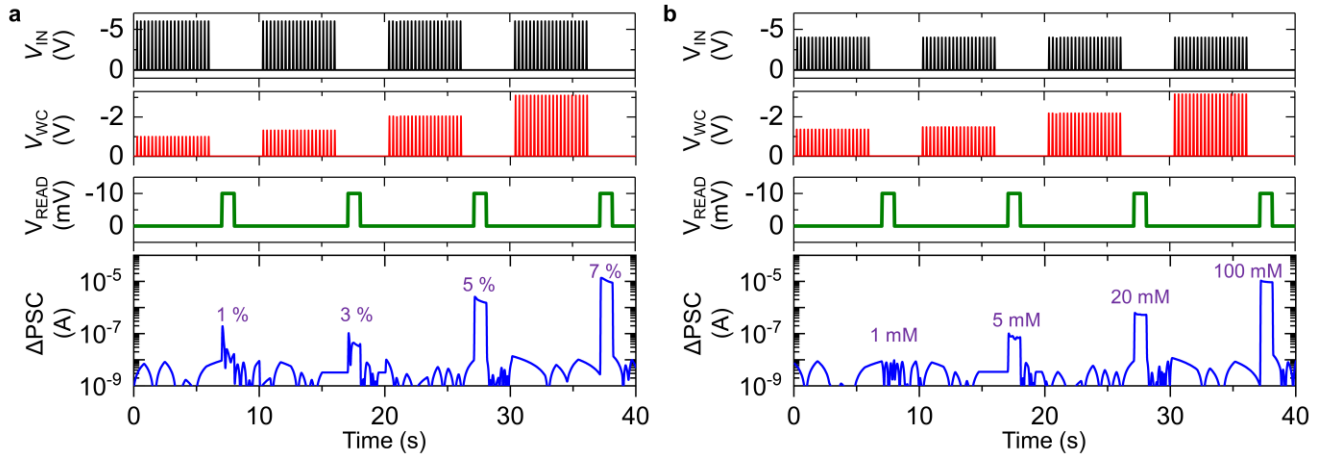
**Supplementary Fig. S11 | Circuit diagrams of the sensor-synapse unit based on a voltage divider.**

**a.** Strain sensor (to simulate the stomach sensor) and **b,** glucose sensor connected to the synapse. The  $V_{wc}$  applied to the synapse is amplified upon stomach expansion and increases glucose level.

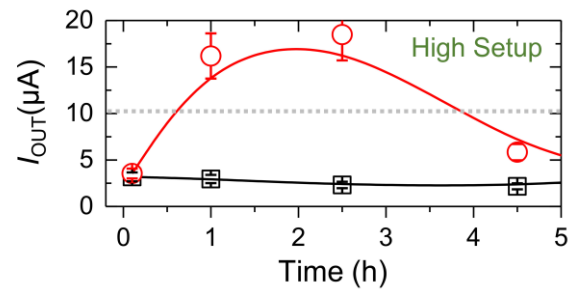
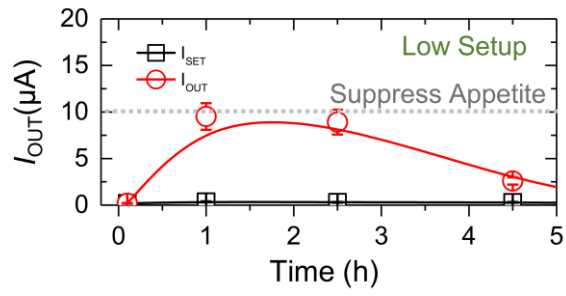


**Supplementary Fig. S12 | The resistance changes of the sensors and resulting  $V_{WC}$  and synaptic current change.**

**a.** Measured  $V_{WC}$  inputs from stomach sensor-synapse unit upon varied mechanical stress. **b.** A plot of resistance and corresponding  $V_{WC}$  as a function of the applied strain. **c.** LTP and retention PSC of the synaptic device connected to the strain sensor under varied strain. **d.** Measured  $V_{WC}$  inputs from the glucose sensor-synapse unit upon varied glucose levels. **e.** A plot of resistance and corresponding  $V_{WC}$  as a function of the glucose level. **f.** LTP and retention PSC of the synaptic device connected to the glucose sensor under varied glucose levels.



**Supplementary Fig. S13 | Real-time plots of  $V_{IN}$ ,  $V_{WC}$ ,  $V_{READ}$ , and corresponding PSC of a sensor-synapse integrated unit. a.** Real-time plots of  $V_{IN}$ ,  $V_{WC}$ ,  $V_{READ}$ , and corresponding PSC of a sensor-synapse integrated device simulating stomach expansion and **b.** increasing glucose level.



**Supplementary Fig. S14 | Retention current of the LTS and read PSC of the appetite control system.** Plots of the set current of LTS (black) and read PSC of the appetite control system in normal and obese cases.